Int. J. Multiphase Flow Vol. 13, No. 1, pp. 57–69, 1987
Printed in Great Britain.

0301-9322/87 $3.00 + 0.00

THE EFFECTS OF SURFACE TENSION AND VISCOSITY ON THE RISE VELOCITY OF A LARGE GAS BUBBLE IN A CLOSED, VERTICAL LIQUID-FILLED TUBE

H. V. NICKENS† and D. W. YANNITELL
Department of Mechanical Engineering, Louisiana State University, Baton Rouge, LA 70803, U.S.A.

(*Received* 5 *September* 1984; *in revised form* 23 *February* 1986)

Abstract—The rise of a large gas bubble or slug through a closed vertial tube of radius R and diameter D containing liquid has been calculated by potential flow theory. The effects of interfacial surface tension are explicitly accounted for by application of the Kelvin–Laplace equation and solving for the bubble shape. The solution is expressed in terms of the Stokes stream function which consists of an infinite series of Bessel functions. The resultant equations have been solved for the first six terms in the series. For negligible surface tension and negligible liquid viscocity, the bubble slip velocity is given by $U_s = 0.352\sqrt{gD}$ and the radius of curvature at the nose $R_c/R = 0.76$. For air/water in a 2.54 cm dia tube, the inclusion of surface tension gives $U_s = 0.346\sqrt{gD}$, $R_c/R = 0.71$, which is consistent with experimental observation. The shape of the gas–liquid interface is hemispherical near the nose for large-diameter tubes, where surface tension is negligible. For small-diameter tubes, however, the surface deviates from hemispherical. It is also shown that for viscous liquids the potential flow solution may be applied with good results to a tube of effective radius $R_{eff} = R - \nu\delta$, where δ is the laminar wall film thickness and ν is a function of the liquid properties and tube size.

INTRODUCTION

The rise of a large gas bubble, or slug, through a vertical duct containing liquid is of practical importance in many disciplines such as nuclear engineering (rod bundles), chemical and mechanical engineering (heat exchangers) and petroleum engineering (gas-lift production).

This problem has been treated theoretically using potential flow theory by several authors (Dumitrescu 1943; Davies & Taylor 1950; Collins 1967; Collins *et al.* 1978). Potential flow theory is valid as long as the liquid viscosity is negligibly small so that the boundary layer at the tube wall will be thin, at least near the bubble nose where the calculations of the bubble shape and drag are critical. In small tubes, however, the curvature of the bubble surface, and therefore the surface tension effects, become significant, In addition, a thin viscous boundary layer at the tube wall can represent a significant fraction of the tube radius, thus decreasing the effective tube diameter.

In this paper the potential flow equations are solved for irrotational inviscid flow of the liquid past the bubble. The bubble shape is an integral part of the solution (as it was in the earlier work cited), but the effect of surface tension on the bubble curvature is accounted for explicitly in the boundary conditions at the gas–liquid interface. The surface tension effects are seen to be significant for Eotvos numbers ($Eo = \rho g D^2/\sigma$) below approx. 70, which corresponds to a tube diameter of about 2.25 cm for air slugs in water.

A viscous correction term is introduced also to account for the decrease in effective tube diameter due to the laminar boundary layer at the tube wall, thus extending the applicability of the solution to liquids of moderate viscosity.

Finally, an easily applied approximation is presented which provides excellent agreement with this analysis and with published experimental data for a wide range of liquid properties and tube diameters.

THE POTENTIAL FLOW MODEL

Figure 1 depicts the basic geometry of the problem. The coordinate system is taken to be attached to the bubble nose, with the z-axis vertically upward, and steady flow of the liquid is assumed

†Present address: Amoco Production Co., Tulsa Research Center, P.O. Box 3385, Tulsa, OK 74102, U.S.A.

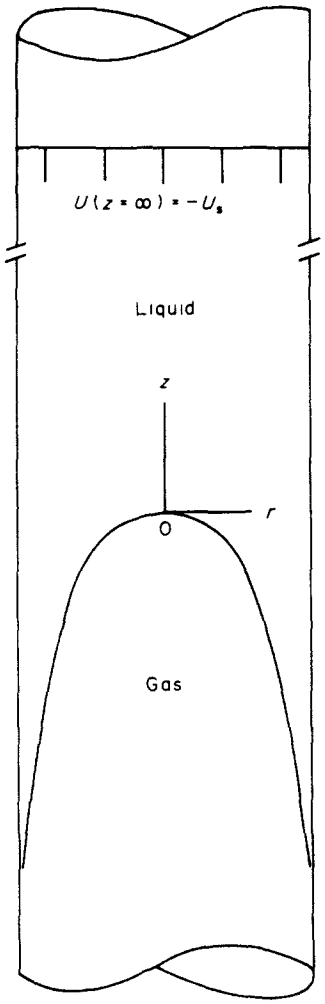

Figure 1. Coordinate system chosen for a gas slug rising in a closed vertical tube of infinite length.

downward over the bubble. A solution of the potential flow equations is sought in terms of the Stokes stream function Ψ, subject to the following boundary conditions:

(i) the top of the tube is assumed closed so that, referred to the bubble frame,

$$\lim_{z\to\infty} u(r, z) = -U_s,$$

where U_s is the rise velocity of the bubble;

(ii) $v(R, z) = 0$ at the solid tube wall;

(iii) $u(0, 0) = v(0, 0) = 0$, since the coordinate origin is a stagnation point;

(iv) the gas–liquid interface (the shape of which is to be determined) is a stream surface, so that the normal component of liquid velocity vanishes and the tangential component will equal that of the gas inside the bubble;

(v) the liquid and gas pressures at the interface are related by the Kelvin–Laplace surface tension equation.

Boundary conditions (i)–(iv) would be sufficient to define the solution in the liquid if the bubble shape were known. Condition (v) is required to determine this shape. The interface conditions (iv) and (v) are developed in the next section.

THE INTERFACE EQUATION

Since the interface is a stream surface one may write Bernoulli's equation on the liquid side as

$$P_L + \tfrac{1}{2}\rho_L V_L^2 + \rho_L g z = P_{LO} \quad [1]$$

and on the gas side as

$$P_G + \tfrac{1}{2}\rho_G V_G^2 + \rho_G g z = P_{GO}, \quad [2]$$

where P is the pressure, ρ is the density, V is the fluid velocity magnitude, subscripts L and G represent liquid and gas, respectively, and subscript O refers to the stagnation point at the origin. At a point on the interface the pressures are related by the Kelvin–Laplace equation,

$$P_G = P_L + \sigma\left(\frac{1}{R_1} + \frac{1}{R_2}\right), \quad [3]$$

where σ is the interfacial surface tension, assumed constant, and R_1 and R_2 are orthogonal radii of curvature of the surface at the point of interest. Combining [1]–[3] and equating gas and liquid velocities provides

$$T_1(r, z) = u^2 + v^2 + 2gz + 2\lambda(K - K_O) = 0, \quad [4]$$

where

$$\lambda = \frac{\sigma}{(\rho_L - \rho_G)} \quad \text{and} \quad K = -\left(\frac{1}{R_1} + \frac{1}{R_2}\right).$$

The requirement that the normal component of velocity vanish at the interface can be written

$$\bar{V}_1 \cdot \nabla H = 0,$$

where $H(r, z) = Z(r) - z = 0$ defines the surface and $\bar{V}_1$ is the liquid velocity vector at the interface. Thus, one can define

$$T_2(r, z) = v\frac{dz}{dr} - u = 0 \quad [5]$$

on the interface $z = Z(r)$.

Equations [4] and [5] thus express boundary conditions (iv) and (v), the only remaining requirement being to relate K in [4] to the interface shape function $Z(r)$. This relation is given as

$$K(r) = \frac{rZ'' + [1 + (Z')^2]Z'}{r[1 + (Z')^2]^{\frac{3}{2}}}, \quad [6]$$

and is derived in Nickens (1986).

THE STREAM FUNCTION

A Stokes stream function Ψ for steady laminar flow around a slug in a closed vertical pipe of radius R is well-known and is given by Collins *et al.* (1978) as

$$\Psi(r, z) = \left[\tfrac{1}{2}r^2 - r\sum_{n=1}^{\infty} d_n J_1(\delta_n r)\exp(-\delta_n z)\right]U_s, \quad [7]$$

where U_s is the bubble slip velocity, d_n and δ_n are constants and J_1 is the first-order Bessel function. Collins considered only the $n = 1$ term in the series. Surface tension and viscous effects were also neglected. Here we shall show the results of taking additional terms into account, as well as the effects of surface tension on the interfacial shape.

Making the convenient definition

$$B_{ij} = \sum_{n=1}^{\infty} d_n \delta_n^j J_i(\delta_n r)\exp(-\delta_n z),$$

[7] becomes

$$\Psi(r, z) = (\tfrac{1}{2}r^2 - rB_{10})U_s. \qquad [8]$$

The radial and axial velocity components are then given, respectively, by

$$v(r, z) = V_r = \frac{1}{r}\frac{\partial \Psi}{\partial z} = -U_s\left(\frac{\partial B_{10}}{\partial z}\right) \qquad [9a]$$

and

$$u(r, z) = V_z = -\frac{1}{r}\frac{\partial \Psi}{\partial r} = U_s\left(\frac{B_{10}}{r} + \frac{\partial B_{10}}{\partial r} - 1\right). \qquad [9b]$$

It may be shown from the properties of Bessel functions that

$$\frac{\partial B_{ij}}{\partial r} = B_{i-1,j+1} - \left(\frac{i}{r}\right)B_{ij}$$

and

$$\frac{\partial B_{ij}}{\partial z} = -B_{i,j+1},$$

so that [9a,b] become

$$v(r, z) = B_{11}U_s \qquad [10a]$$

and

$$u(r, z) = (B_{01} - 1)U_s. \qquad [10b]$$

Boundary conditions (ii) and (iii) now require that

$$\sum_{n=1}^{\infty} d_n\delta_n J_1(\delta_n R)\exp(-\delta_n z) = 0 \qquad [11a]$$

and

$$\sum_{n=1}^{\infty} d_n\delta_n = 1. \qquad [11b]$$

For [11a] to be satisfied for all z requires that

$$J_1(\delta_n R) = 0$$

and thus

$$\delta_n = \frac{k_n}{R},$$

where k_n is the nth zero of J_1.

Since Ψ consists of an infinite series, the solution is approximated by truncating the series after some N terms, herein referred to as the Nth-order approximation. Such an approximation requires the determination of N constants d_n and the unknown slip speed U_s. The $(N + 1)$ simultaneous equations are provided by [11b] and the interface equations [4] and [5], as described in the following section.

THE SOLUTION OF THE INVISCID EQUATIONS

The functions T_1 and T_2 as defined by [4] and [5] are identically zero everywhere on the gas–liquid interface; it therefore follows that their total derivatives of any order are also zero on the interface. The total derivative of a function $T(r, z)$ on the interface is defined as

$$\frac{DT}{Dr} = \frac{\partial T}{\partial r} + \frac{\partial T}{\partial z}\frac{\partial z}{\partial r} = \frac{\partial T}{\partial r} + Z'\frac{\partial T}{\partial z}.$$

Thus, the derivatives of u and v are determined from [10a,b] those of Z from [5] and those of K from [6]. These are substituted into the derivatives of T_1, using [4], which are evaluated at the stagnation point. Since the number of these equations required increases with the order of the approximation, the analysis becomes very complicated for higher order solutions. The calculations have been performed for orders up to $N = 6$ and the details are presented in Nickens (1986). Only the second-derivative equations will be presented here as an example.

Defining

$$Z_m = \frac{\mathrm{d}^m Z}{\mathrm{d}r^m} \quad \text{and} \quad \phi_{mn} = \frac{\partial^{(m+n)}\phi}{\partial r^m \partial z^n},$$

where ϕ is any function $\phi(r, z)$, it may be shown that

$$(u_{mn})_O = \tfrac{1}{2}(-1)^{(\frac{m}{2}+n)} C_n^m (B_{0,m+n+1})_O \qquad [12a]$$

and

$$(v_{mn})_O = \tfrac{1}{2}(-1)^{(\frac{m-1}{2}+n)} C_{n+1}^m (B_{0,m+n+1})_O, \qquad [12b]$$

where

$$C_a^b = \frac{b!}{a!(b-a)!}.$$

Noting that the axial symmetry of the bubble requires that all odd derivatives of $Z(r)$ vanish at $r = 0$, we can also show that the second total derivative along the interface of any function $T(r, z)$ is given by

$$\left(\frac{\mathrm{D}^2 T}{\mathrm{D}r^2}\right)_O = (T_{20} + T_{01} Z_2)_O.$$

Thus, using T_2, from [5], in the above we find that

$$(Z_2)_O = \left(\frac{u_{20}}{2v_{10} - u_{01}}\right)_O = \left(\frac{-B_{03}}{4B_{02}}\right)_O.$$

and, from [6],

$$(K_2)_O = -(4Z_2^3 - \tfrac{4}{3}Z_4)_O.$$

Finally, from [4],

$$\left(\frac{\mathrm{D}^2 T_1}{\mathrm{D}r^2}\right)_O = (v_{10}^2 + gZ_2 + \lambda K_2)_O = 0. \qquad [13]$$

THE FIRST-ORDER APPROXIMATION

An analytical solution is possible only for the first approximation, $N = 1$. In this case [11a,b] give

$$d_1 \delta_1 = 1 \quad \text{or} \quad d_1 = \frac{R}{k_1}.$$

In addition, [12a,b] provide

$$(v_{10})_O = \left(B_{02} - \frac{B_{11}}{r}\right)_O U_s = \tfrac{1}{2} U_s (B_{02})_O = \frac{d_1 \delta_1^2 U_s}{2},$$

$$(u_{20})_O = \left(\frac{B_{12}}{r} - B_{03}\right)_O U_s = -\tfrac{1}{2} U_s (B_{03})_O = \frac{d_1 \delta_1^3 U_s}{2}$$

and

$$(u_{01})_O = -(B_{02})_O U_s = -d_1 \delta_1^2 U_s,$$

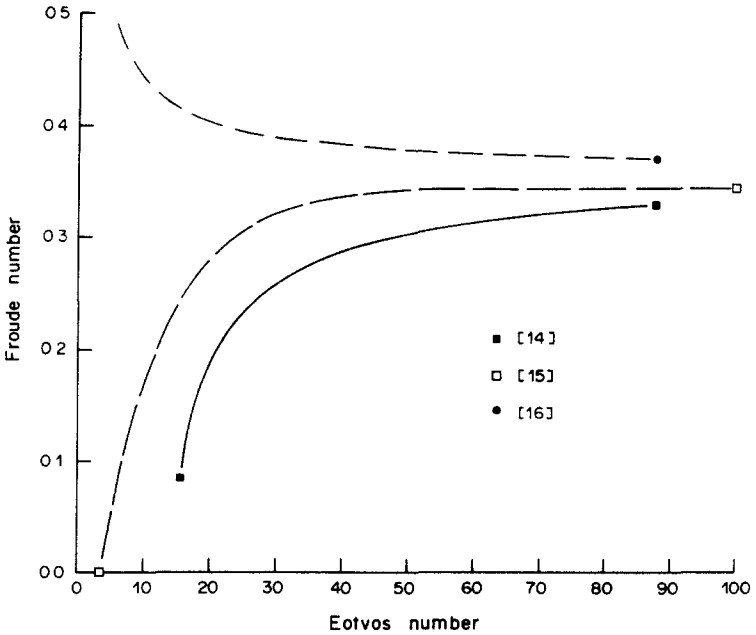

Figure 2. Calculated Fr vs Eo for air/water ($N = 1$).

where use has been made of the relation

$$\lim_{r\to 0} 0\left(\frac{B_{ij}}{r}\right) = \tfrac{1}{2}B_{0,j+1}.$$

In the analysis the shape of the bubble is expanded in a Taylor series about the origin (bubble nose). If the series approximation for the bubble shape $Z(r)$ is also truncated after just one term, [13] then becomes

$$\left(\frac{U_s^2 B_{02}}{4} - \frac{gB_{03}}{4B_{02}} + \frac{\lambda B_{03}^2}{16B_{02}^3}\right)_0 = 0.$$

Defining the Eotvos number,

$$\mathrm{Eo} = \frac{4gR^2}{\lambda} = \frac{4gR^2(\rho_L - \rho_G)}{\sigma},$$

and solving for the slip speed gives

$$U_s = \left[\frac{gR}{k_1}\left(1 - \frac{k_1^2}{\mathrm{Eo}}\right)\right]^{\frac{1}{2}} = 0.361\sqrt{2gR}\left(1 - \frac{14.68}{\mathrm{Eo}}\right)^{\frac{1}{2}}. \qquad [14]$$

It can be seen immediately that [14] predicts a Froude number,

$$\mathrm{Fr} = U_s/\sqrt{2gR},$$

which approaches a constant value of 0.361 for large Eotvos numbers (negligible surface tension). This is in agreement with the Collins *et al.* (1978) one-term solution which neglects surface tension. The equation also predicts the correct trend for lower values of Eo, as observed experimentally (Wallis 1962; White & Beardmore 1962; Harmathy 1960). Figure 2 shows [14] compared with the experimental correlation

$$\mathrm{Fr} = 0.345\left[1 - \exp\left(\frac{3.37 - \mathrm{Eo}}{10}\right)\right], \qquad [15]$$

given by Wallis (1962), which is known to agree well with experimental observation of a variety of gas/liquid systems, provided the viscous effect is negligible. Although the trend is correct, the agreement is not especially good. (It should be noted here that [15] is a reasonable correlation for

actual data which exhibit normal experimental scatter. It would be unrealistic to expect exact agreement of theory to this curve.)

It is not necessary to truncate the Taylor series after one term. If the Z_4 term is computed from [5] and used in [13] the result (after some algebra) is given by

$$U_s = 0.361\sqrt{2gR}\left(1 + \frac{4.89}{\text{Eo}}\right)^{\frac{1}{2}}, \qquad [16]$$

which has the same asymptote for large Eo but exhibits the wrong trend at lower values. Additional terms in the series have no effect on the equations for $N = 1$. In fact, for general N, only $N + 1$ terms of the Taylor series appear in the equations. Since all odd terms are identically zero, by symmetry, the order N_D of the shape series is at most $2(N + 1)$.

As stated in the next section, it was found that inclusion of more than $N + 2$ terms in the Taylor series caused deterioration in the quality of the results, indicating that the truncation of the shape series should be kept consistent with that of the Bessel function series.

HIGHER ORDER APPROXIMATIONS

For $N > 1$ no analytic solutions are readily available, and a multidimensional Newton–Raphson technique, described in Nickens (1986), was used to solve the equations numerically. The case $N = 2$ is of some interest as it can be proved that, for $\text{Eo} = \infty$, only one real solution exists. That solution was determined to be, for a tube of radius 1.27 cm,

$$d_1 = 0.1717, \quad d_2 = -0.0225, \quad U_s = 14.45 \text{ cm/s}, \quad \text{Fr} = 0.29;$$

which is not consistent with either experimental observation or the numerical solutions for larger N.

For $N = 3$, $N_D = 4$, a solution was obtained which agrees well with the empirical correlation equation, as shown in figure 3. With N_D increased to 6, the numerical solution agrees even better in the asymptote as $\text{Eo} \to \infty$, but exhibits the wrong behavior for low Eotvos numbers (high surface tension).

As N is increased further this trend continues. At large Eotvos numbers ($\text{Eo} > 70$) the bubble velocity converges very well to the experimental values as N_D is increased to $2(N + 1)$ (figure 4). At low Eotvos numbers, however, the solutions given by $N_D = N + 1$ (for odd N) or $N_D = N + 2$

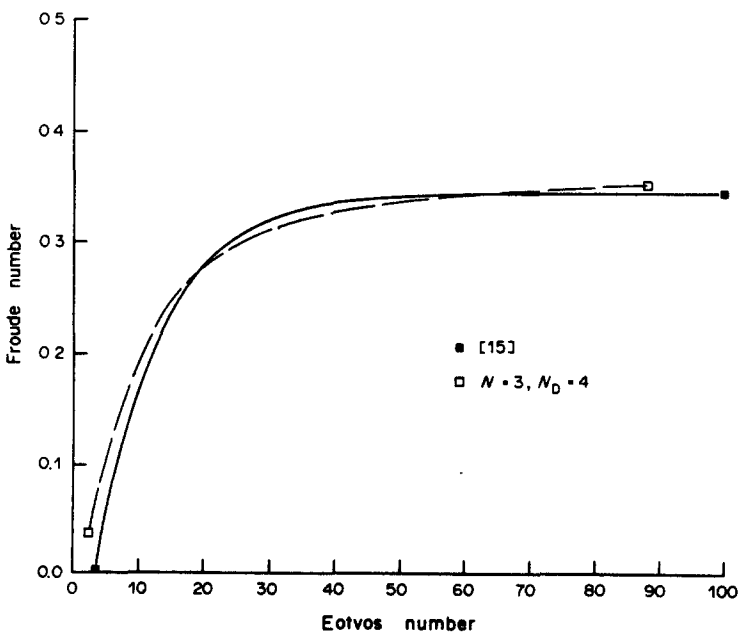

Figure 3. Calculated Fr vs Eo for air/water ($N = 3$, $N_D = 4$).

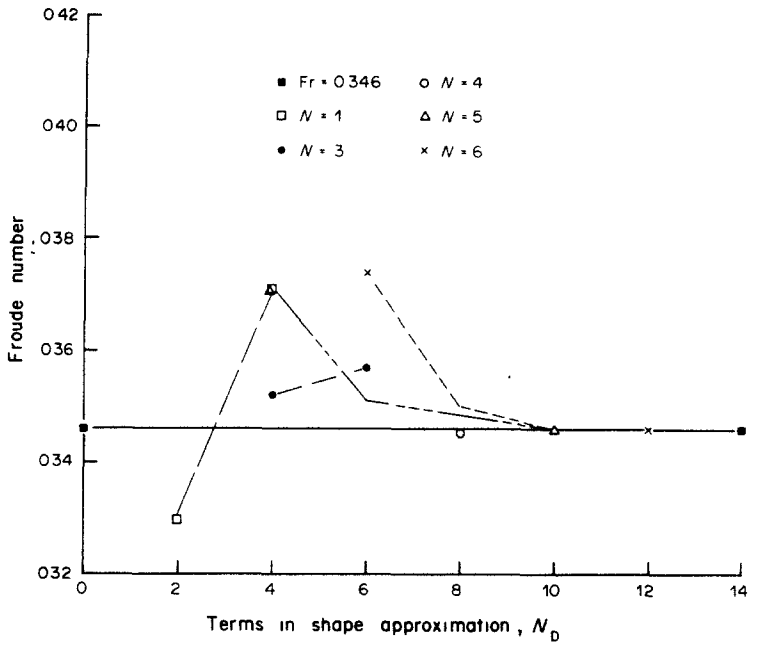

Figure 4. Calculated Fr for air/water showing convergence as additional terms are included in the series expansion.

(for even N) produce the best agreement. In fact, these solutions are almost indistinguishable from the $N = 3$, $N_D = 4$ solution.

BUBBLE-SHAPE CALCULATION

The bubble shape near the nose is readily calculated from [8] by requiring $\Psi = 0$ at the gas–liquid interface.

For an air/water system in a tube of radius $R = 1.27$ cm (Eo = 88), the radius of curvature R_c at the nose rapidly converges to a value of $0.71R$ as N and N_D are increased. For negligible surface tension, the solutions converge to $R_c/R = 0.76$.

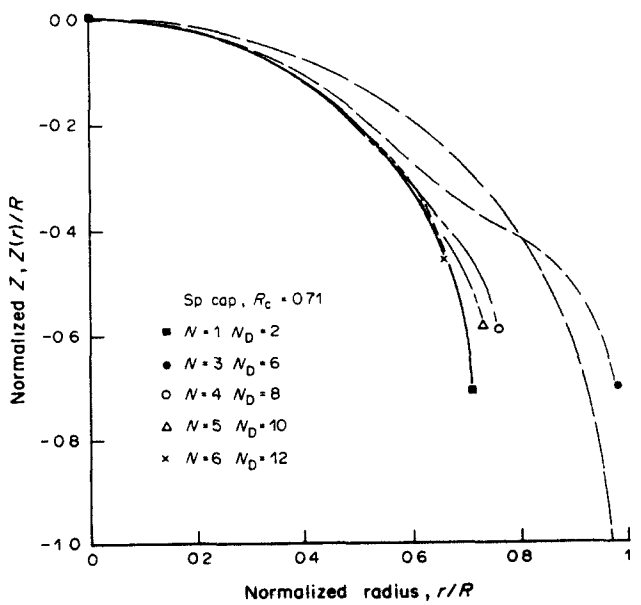

Figure 5. Calculated bubble shape compared to "spherical cap" for air/water in a 2.54 cm dia tube.

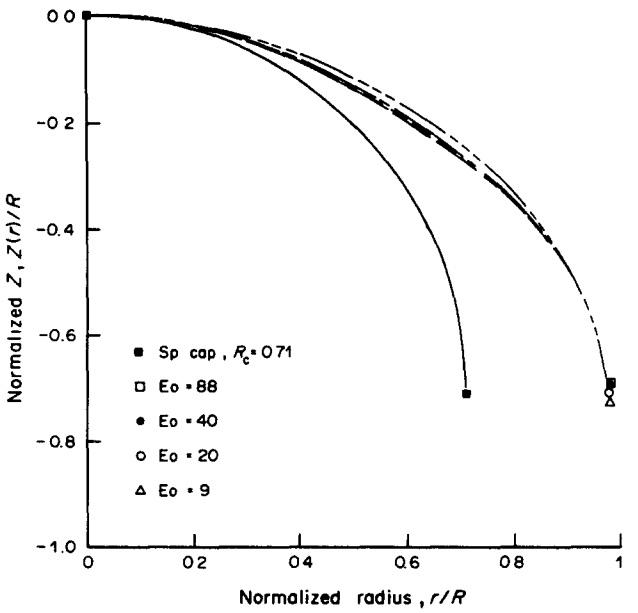

Figure 6. Effects of surface tension on bubble shape for air/water ($N = 3$, $N_D = 4$).

Figure 5 compares the calculated bubble shape for air/water in a tube of radius 1.27 cm with a spherical cap of radius $0.71R$ for various values of N ($N_D = 2N$). It is clear that the bubble shape approaches the spherical cap as N is increased. This supports the assumption of previous authors that the interface assumes a spherical shape near the nose. In fact, it can be proven (Nickens, 1986) that, for negligible surface tension, the bubble shape must, out of necessity, be hemispherical near the nose. As surface tension effects become more significant (Eo < 40) the shape of the interface deviates from hemispherical as surface tension forces begin to dominate.

Figures 6 and 7 illustrate the effects of surface tension on the $N = 3$, $N_D = 4$ and $N = 5$, $N_D = 6$ solutions. Although the lack of convergence of the bubble shape at these values of N produces some oddities far from the nose, the important feature is the increased bluntness of the bubble near the nose. This blunting of the nose results in a decrease of the rise velocity and is a direct result of the surface tension.

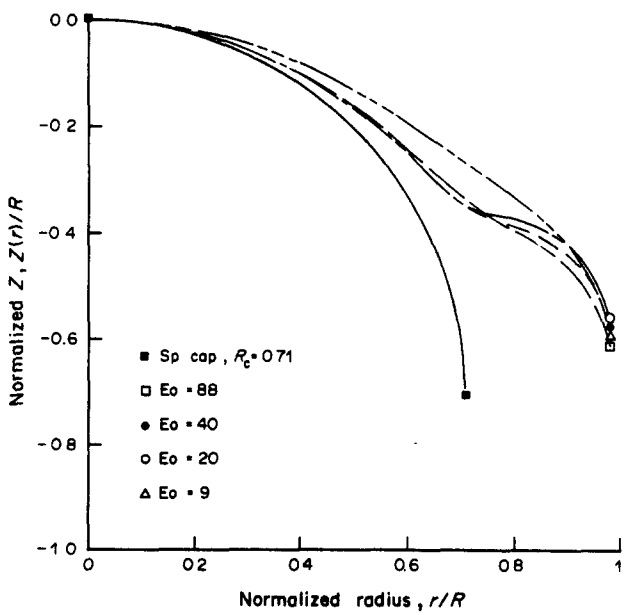

Figure 7. Effects of surface tension on bubble shape for air/water ($N = 5$, $N_D = 6$).

CORRECTION FOR SMALL LIQUID VISCOSITY

Although the liquid viscosity cannot be accounted for directly by potential flow theory, a simple approximation of the viscous effects for small viscosity is to estimate the reduction of the effective tube radius caused by the boundary layer at the tube wall. It is still assumed that the boundary layer at the gas–liquid interface is negligible in comparison to that at the tube wall.

Potential theory requires that the bubble surface approach the tube wall asymptotically as z becomes negative infinite. However, the actual bubble is confined within the radius $R - \delta$, where δ is the thickness of the fully developed laminar liquid film. The boundary-layer thickness must increase from zero at large positive z to δ at large negative z. Potential theory applies only in the liquid region between the boundary layer and the bubble.

The above potential flow theory may be applied to predict the rise velocity in a viscous liquid by utilizing the effective tube radius

$$R_{\text{eff}} = R - v\delta, \tag{17}$$

where $0 \leqslant v \leqslant 1$ and v depends on the liquid properties.

Straightforward application of mass and momentum balance to the fully developed laminar liquid film (at large negative z) yields the relation

$$U_s = \frac{2\eta R^2}{3} \frac{\epsilon^3}{1-\epsilon} \tag{18}$$

between the bubble slip speed and the film thickness. Here $\epsilon = \delta/R$ is the nondimensional film thickness and $\eta = \rho g/\mu$ is a measure of the liquid properties. Equation [18] provides an additional constraint on the above solution and imposes the additional unknown ϵ. It is derived in detail in Nickens (1984) and is also given by Brown (1965).

There remains, of course, the parameter v to be determined. Physically one would expect an ideal liquid to have $v = 0$ (no boundary layer) and that v should, in general, increase with viscosity. The resulting theory is shown to apply for viscosities up to a maximum at which $v = 1$. Beyond this the boundary layer is apparently thicker than the fully developed film and a truly viscous analysis is required (i.e. the potential theory fails).

A PRACTICAL METHOD

The above $N = 3$, $N_D = 4$ solution has been shown to provide very good agreement with observed data. Assuming that the general shape of the solution curve for $\text{Eo} < 100$ is correct, this agreement can be enhanced slightly by adjusting the asymptote to that predicted by the $N = 6$, $N_D = 12$ solution for large Eo and negligible liquid viscosity. The predicted value of $\text{Fr} = 0.352$ under these conditions is nearly identical to that of Dumitrescu (1949).

A good approximation to the resulting curve is then given by

$$\text{Fr} = 0.352\left(1 - \frac{3.18}{\text{Eo}} - \frac{14.77}{\text{Eo}^2}\right) \tag{19}$$

for negligible viscosity. To include the effect of viscosity, as in the preceding section, [19] may be modified to

$$\text{Fr} = 0.352 R_N^{\frac{1}{2}}\left(1 - \frac{3.18}{R_N^2 \text{Eo}} - \frac{14.77}{R_N^4 \text{Eo}^2}\right), \tag{20}$$

where $R_N = R_{\text{eff}}/R$ is the normalized effective tube radius.

Here it is assumed that v is an exponential function of the nondimensional liquid property number,

$$N_p = \left(\frac{\rho^2 g R^3}{\mu^2}\right)_L^{\frac{1}{2}}.$$

Table 1. Details of the fluids used by White & Beardmore (1962)

Fluid	Temperature (°C)	ρ (g/ml)	μ (cP)	σ (dyn/cm)
Distilled water	26	0.997	0.87	71.5
40% Sucrose solution	26	1.172	5.65	77.7
58% Sucrose solution	25	1.272	40.50	76.0
Ethylene glycol	26	1.113	19.9	47.5
Aqueous ethanol	26	0.803	1.385	22.8
Tellus oil	25	0.864	52	31.0
Voluta oil	25	0.902	294	30.8
Glycerol	24	1.260	712	63.1
90% Glycerol solution	24	1.234	154	64.8
95% Glycerol solution	25	1.246	323	63.9
Sugar syrup	27	1.42	20,900	77.2
Diluted sugar syrup	27	1.40	2650	77.0
Rediluted sugar syrup	26	1.39	1610	76.9

A fit of [20] to the data of table 1 and figure 7 of Tellus oil at Eo = 30 and Eo = 100 yields the expression

$$v = 6.40 N_p^{-0.60}. \qquad [21]$$

The minimum N_p for which [20] should be valid is then $N_p = 22$ (i.e. $v = 1$).

Applying this analysis to several of the liquids of table 1 produces the results in figure 8, which compare favorably with the experimental data of White & Beardmore (1962), reproduced in figure 9, for Eotvos numbers as low as 8 for the low-viscosity liquids. As intuitively expected, the Eotvos number below which good agreement is obtained increases with viscosity. The filled circles in figure 6 denote the value of Eo at which $N_p = 22$ for each liquid, if this value exceeds the minimum Eo at which Fr = 0. It can be seen that agreement is very good for Eo above the filled circles but begins to deteriorate at lower values of Eo.

Values of R_N have been calculated for a variety of liquid properties and the results presented in figure 10 as a function of Eo. If the liquid properties and tube radius are given, figure 8 and [20] may be easily utilized to predict the bubble velocity.

For example, consider a solution of 58% sucrose in water, with properties as given in table 1, in a tube of dia 1.27 cm. Thus $N_p = 50$, Eo = 26.5 and R_N, obtained from figure 10, is 0.875.

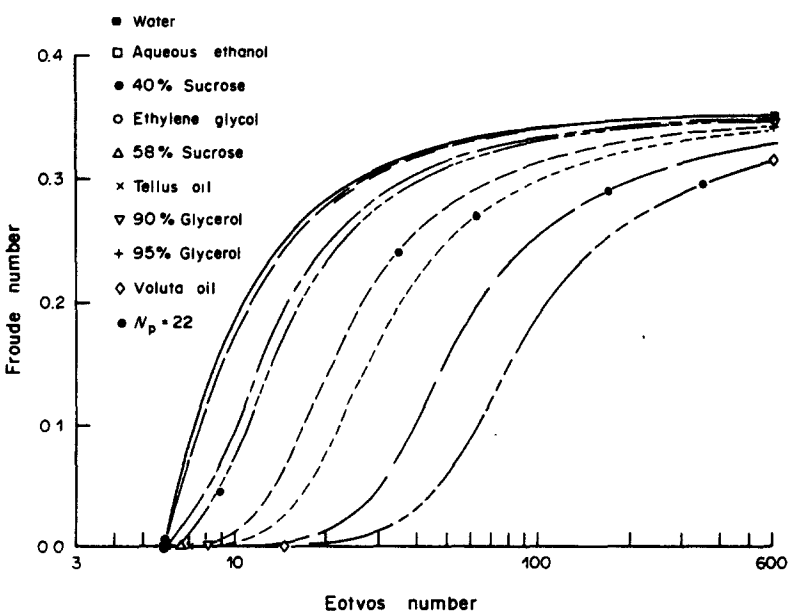

Figure 8. Calculated Fr vs Eo for viscous liquids using effective diameter.

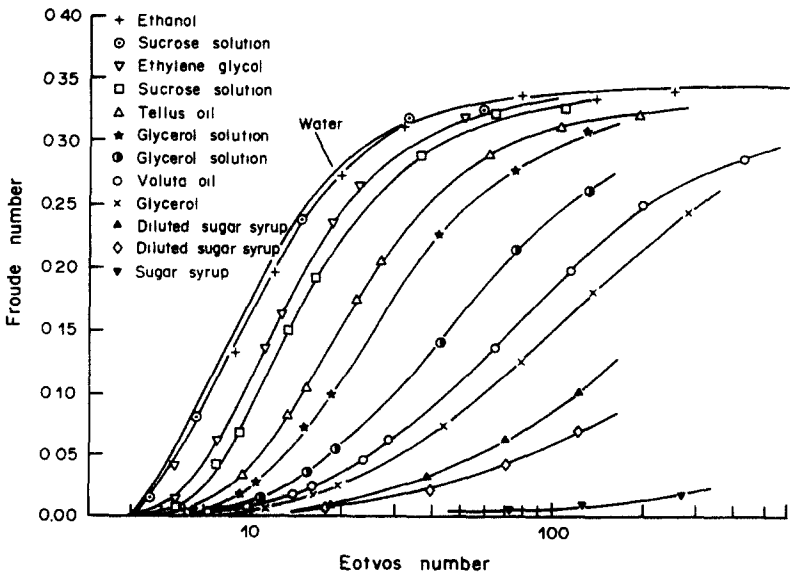

Figure 9. Measured Fr vs Eo for viscous liquids (White & Beardmore 1962).

Equation [20] then yields $\mathrm{Fr} = 0.265$ and the bubble slip velocity $U_s = 9.35$ cm/s. This value compares well with the experimental data of figure 9.

Figure 11 graphically summarizes the results of the viscous approximation theory. This figure may also be used in place of figure 8 and [20], although it is more difficult to interpolate at low values of N_p. A computer program is also provided in Nickens (1986) that solves the equations for R_N and predicts the Froude number and velocity directly.

CONCLUSIONS

The potential flow analysis of large bubbles in liquid-filled tubes has been extended to account for surface tension effects at the liquid–gas interface, thus allowing its application to small-diameter

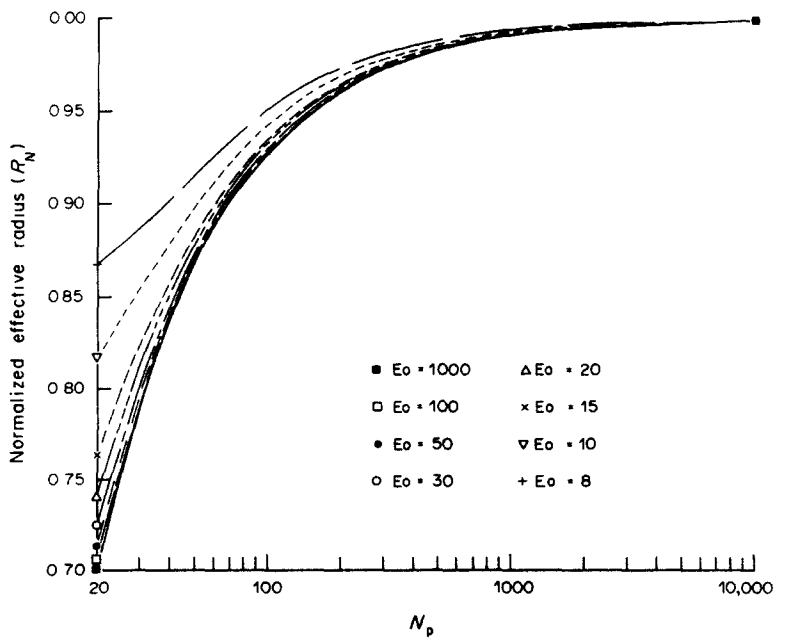

Figure 10. Normalized effective radius as function of Eo and the liquid property number N_p.

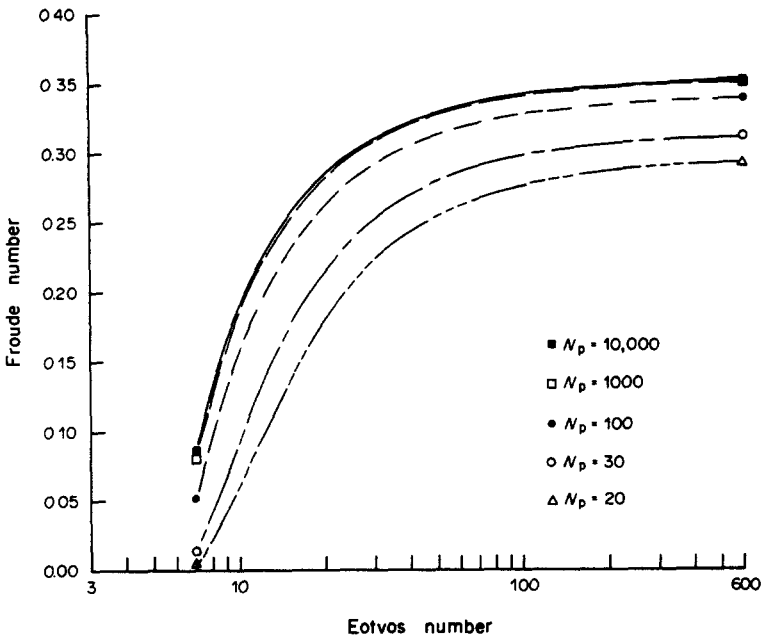

Figure 11. Calculated Fr vs Eo as function of the liquid property number N_p.

tubes where the bubble curvature is large and surface tension forces begin to dominate inertial forces. This required the inclusion of more terms in the series expansion for the velocity potential than previously published works have provided, as well as an explicit calculation of the bubble shape.

In addition, the effect of moderate liquid viscosity may be approximated by replacing the actual tube diameter with an effective diameter which accounts for the thin boundary layer at the tube wall. This approximation has been shown to agree well with published experimental data for a considerable range of tube sizes and liquid properties.

REFERENCES

BROWN, R. A. S. 1965 The mechanics of large gas bubbles in tubes. I. Bubble velocities in stagnant liquids. *Can. J. chem. Engng* **43**, 217–223.

COLLINS, R. 1967 The effect of a containing cylindrical boundary on the velocity of a large gas bubble in a liquid. *J. Fluid Mech.* **28**, 97–113.

COLLINS, R., DEMORAES, F. F., DAVIDSON, J. F. & HARRISON, D. 1978 The motion of a large gas bubble rising through liquid flowing in a tube. *J. Fluid Mech.* **89**, 497–514.

DAVIES, R. M. & TAYLOR, G. 1950 The mechanics of large bubbles rising through extended liquids and through liquids in tubes. *Proc. R. Soc., A* **200**, 375–390.

DUMITRESCU, D. T. 1943 Strömung an einer Luftblase im senkrechten Rohr. *Z. angew. Math. Mech.* **23**, 139–149.

HARMATHY, T. Z. 1960 Velocity of large drops and bubbles in media of infinite or restricted extent. *AIChE Jl* **6**, 281–288.

NICKENS, H. V. 1986 The velocity and shape of gas slugs rising in vertical tubes and rectangular slots. Ph.D. Dissertation, Louisiana State Univ., Baton Rouge, La.

WALLIS, G. B. 1962 General correlations for the rise velocity of cylindrical bubbles in vertical tubes. Report 62GL130, General Engineering Lab., General Electric Co., Schenectady, N.Y.

WHITE, E. T. & BEARDMORE, R. H. 1962 The velocity of rise of single cylindrical air bubbles through liquids contained in vertical tubes. *Chem. Engng Sci.* **17**, 351–361.